Influence of heat treatment on the microstructure, phase transformation, and thermal cycling stability of NiTiZr alloys

Qiang Yu [1], Rizawanguli[1], Pengfei Qi [1], Ruixin Gong [2] , Qian Zhang[3], and Wentao Qu[3]*

[1] School of Intelligent Transportation, Xinjiang Vocational University, Urumqi 830000,China
[2] College of Petroleum Engineering, Xi'an Petroleum University Engineering Research Center of Safety and Energy Saving in Oil & Gas Storage and Transportation, Universities of Shaanxi Province,710065, China
[3] School of Mechanical Engineering, Xi'an Petroleum University, Xi'an, Shaanxi, 710065,China

(Received 06 March 2026; Accepted 28 July 2026)

Abstract: This work examines how the post-annealing temperature affects the thermal-energy storage behavior of the Ni49.5Ti38.5Zr12 phase-change alloy, with the aim of mitigating heat loss and electronic failures that often occur in insulation bottles due to structural imperfections or inadequate heat-storage capability. Specimens were heat-treated over a range of temperatures, and their transformation characteristics, microstructural evolution, and thermophysical performance were systematically evaluated. The results indicate that with increasing heat-treatment temperature, the transformation enthalpy rises initially and then declines. This trend is associated with the progressive morphological change of the precipitated λ1 phase-from fine bubble-like features to sheet-like structures-together with a grain size variation that also increases first and subsequently decreases. In addition, thermal conductivity shows an overall upward tendency, which can be explained by enhanced atomic motion in the crystal lattice at elevated temperatures. After annealing at 600 °C, the alloy exhibits a transformation enthalpy of 29.8 $J \cdot g^{-1}$, a transformation start temperature (As) of 72.97 °C, a finish temperature (Af) of 119.81°C, a thermal conductivity of 15.3 $W \cdot g^{-1} \cdot K^{-1}$, and a microhardness of 355.147 HV. Moreover, the material retains good thermal stability after repeated thermal cycling. These outcomes provide theoretical support for employing NiTiZr-based materials in downhole insulation bottles. An annealing window of 500-700 °C is recommended to improve transformation stability and thermophysical properties, enabling suitability for high-temperature service environments such as downhole tools in the petroleum industry.

Keywords: NiTiZr alloy; Heat treatment; Microstructure Phase change characteristics; Thermal cycling stability

1. Introduction

As petroleum exploration and production move toward deep and ultra-deep wells, downhole tools are required to withstand increasingly severe temperature-and-pressure conditions [1-3]. During drilling and oil production, insulation bottles are indispensable for maintaining normal downhole tool operation, avoiding crude-oil solidification, and preserving fluid mobility [4-7]. However, conventional sealing materials in insulation bottles often suffer creep relaxation and lose sealing

integrity at elevated temperatures, creating a need for smart materials that can function reliably under harsh service conditions [8, 9]. Owing to their shape-memory and superelastic responses and their transformation temperatures far higher than those of conventional NiTi, NiTiZr high-temperature shape memory alloys (SMAs) are considered promising candidates for sealing elements in downhole insulation bottles[10, 11].

Ti-Ni SMAs are among the most widely studied functional alloys and have been extensively used in aerospace, biomedical, and other applications [12, 13]. Nevertheless, the martensitic phase transition temperature of conventional binary NiTi alloys is typically below 100 °C, greatly limiting their application in high-temperature downhole environments (typically 100-200 °C or even higher) [14, 15] . To extend the temperature range of application, researchers have developed alloy designs by adding a third element. One of those is zirconium (Zr), which is being widely studied due to its ability to significantly increase the alloy's phase transition temperature [16-18]. It has been reported that forming a NiTiZr ternary alloy by adding an appropriate amount of Zr to Ti-Ni not only preserves the excellent shape-memory ability and superelastic properties of binary NiTi, but also shifts the transformation temperature above 150 °C, meeting the requirements of most downhole conditions [18].

In downhole insulation bottles, sealing components must maintain a stable contact pressure over long durations at high temperature, and the transformation behavior of NiTiZr alloys therefore has a direct influence on sealing performance [19]. In particular, factors such as transformation temperature, hysteresis, and cyclic stability govern the reliability and long-term durability of seals under temperature fluctuations [20]. It is worth noting that the phase transition characteristics of NiTiZr alloys are not fixed but strongly depend on their microstructure, especially the morphology, size, and distribution of precipitates, which are mainly regulated through heat treatment processes [19-22].

NiTiZr alloys undergo significant changes in microstructure under different heat treatment conditions, directly affecting their phase transition characteristics. Studies have shown that changes in annealing temperature can cause significant alterations in the alloy's microstructure [23-26]. For Ti-50.8Ni-0.1Zr, increasing the anneal from 350 to 700 °C converts the morphology from fibrous to equiaxed, and the recrystallization temperature has been reported to lie in the 550 to 600 °C range [27]. Such microstructural changes affect grain-boundary resistance and the driving force for phase transformation, thereby altering transformation behavior. Likewise, raising the aging temperature from 300 to 600 °C leads to substantial changes in the morphology and spatial distribution of Ti3Ni4 precipitates [28]. Specifically, as the aging temperature increases, the Ti3Ni4 precipitates grow from fine particles to lens-shaped structures and ultimately form coarse plate-like structures [29-31]. These precipitates, as microscopic stress fields, interact with martensitic variants, affecting the phase transition process [32]. In alloys with higher Zr content (such as $Ti_{30}Ni_{50}Zr_{20}$), after 1 hour of annealing at 700 °C, the room temperature microstructure consists of lath martensite and λ_1 phase, with a (011) I-type twin relationship between the parallel laths [33]. This complex microstructure further increases the diversity of the phase transition behavior. Heat treatment processes not only affect the microstructure of NiTiZr alloys but also significantly alter their phase transition temperatures and phase transition sequences. As the annealing temperature increases, the phase transition types of Ti-50.8Ni-0.1Zr alloy during cooling/heating show regular changes: from the "A→R→M/M→R→A" type phase transition at low annealing temperatures (A-matrix phase B2; R-R phase; M-martensitic B19'), it gradually transforms into the "A→R→M/M→A" type phase transition at medium annealing temperatures, and finally to the "A→M/M→A" type phase transition at high annealing temperatures [34]. This change clearly reflects the heat treatment's role in regulating the phase transition path. At the same time, with the increase in annealing temperature, both the phase transition temperature and thermal hysteresis show a decreasing trend. This change is closely related to the alterations in defect

density and stress state within the alloy [32]. As the aging temperature increases and aging time is extended, the phase transition behavior of alloys also exhibits regular changes: the 300 °C-aged alloy maintains the "A→R→M/M→R→A" type phase transition; the 400 °C-aged alloy transitions from the "A→R→M/M→R→A" type to the "A→R→M/M→A" type; while the 500 °C and 600 °C-aged alloys show the "A→R→M/M→A" and "A→M/M→A" type phase transitions, respectively [28].

Currently, systematic research on the phase transformation stability of heat-treated NiTiZr alloys in specific downhole petroleum environments remains limited. Therefore, in this work Ni49.5Ti38.5Zr12 was heat-treated at several temperatures to clarify how heat-treatment temperature affects microstructure, transformation characteristics, and thermal-cycling stability, and to further assess its suitability for petroleum-well applications.

2. Experimental Methods

2.1 Materials and heat-treatment procedure

Ni49.5Ti38.5Zr12 alloy was prepared following procedures reported previously. $Ni_{49.5}Ti_{38.5}Zr_{12}$ alloy button ingots were fabricated by arc melting under argon protection using high-purity Ni (99.99%), Ti (99.98%) and Zr (99.99%) elements as raw materials. To ensure homogeneity of the material composition, the ingots were repeatedly melted at least six times. The button ingots were then sealed into quartz tubes filled with argon gas and homogenized at 1223 K for 2 h, followed by water cooling. The specimens were annealed in a muffle furnace at 500 °C, 600 °C, 700 °C, and 800 °C for 30 mins (one set for each temperature). After heating, samples were removed and immediately water-quenched, producing alloys corresponding to different annealing temperatures.

2.2 Microstructural characterization

Phase identification was performed by X-ray diffraction (XRD) using a Rigaku diffractometer (D8 Advance) with Cu-Kα radiation. The optical microscopy (OM) observation was carried out using an OLYMPUS BX51 microscope. Elemental compositions of selected regions were measured with an energy-dispersive spectroscopy (EDS) detector. Surface morphology was observed by scanning electron microscopy (SEM; Zeiss Gemini 360). Prior to SEM observation, specimens were ground sequentially with SiC papers (400 - 3000 grit) until a scratch-free surface was achieved, ultrasonically cleaned in acetone and ethanol for 10 mins, dried with cold air, and finally etched using Kroll's reagent (5 mL HF, 25 mL HNO_3, and 50 mL H_2O).

2.3 Evaluation of thermophysical properties

2.3.1 Density measurement

Density was determined by the Archimedes method. Specimens (10 × 10 × 1.5 mm^3) were weighed in air (wa) and then weighed again while immersed in water (ws). The density was calculated by $\rho = \rho w \cdot wa/(wa - ws)$, where ρw denotes the density of water.

2.3.2 Measurement of phase transition temperatures and thermophysical parameters

Transformation temperatures and transformation enthalpy were measured by differential scanning calorimetry (DSC25) at a heating/cooling rate of 20 °C min^{-1} over -40 to 450 °C. The specific heat capacity (Cp) was obtained using modulated DSC, with sapphire (known Cp) serving as the reference standard. Thermal-cycling stability of Ni49.5Ti38.5Zr12 phase change material (PCM) was evaluated by DSC through 100 consecutive heating-cooling cycles between -40 and 130 °C at 10 °C min^{-1}.

2.3.3 Thermal conductivity and hardness measurements

Thermal diffusivity (α) was measured via the laser-flash technique (NETZSCH LFA467) using square specimens of 10 × 10 × 1.5 mm^3. Measurements were conducted during heating over a temperature range of -50 to 150 °C, covering the phase-change interval, and the thermal cycling test was repeated for 50 heating-cooling cycles. Thermal conductivity was then calculated using $k = Cp \cdot \rho \cdot \alpha$, where Cp, ρ, and α represent specific heat capacity, density, and thermal diffusivity, respectively. Vickers hardness was measured on an HV-50A tester under a 100 N load with a 15 s dwell time.

3. Results and discussion

3.1 Analysis of microstructural morphology

Fig. 1 presents the room-temperature XRD patterns of the Ni49.5Ti38.5Zr12 alloy in the as-homogenized condition and after annealing at different temperatures. All samples contain B2, B19′, NiZr, and $(Ti, Zr)_2Ni$ phases. The coexistence of a B2/B19′ matrix with Zr- or Ni-rich secondary phases is consistent with recent research on Ni-rich NiTiZr alloys, where H/λ-type precipitation and matrix compositional redistribution are closely related to heat-treatment conditions [35]. After annealing, an additional λ1 phase is detected, which corresponds to a TiNiZr ternary solid solution with a C14-type Laves structure. A weak diffraction peak at approximately 41.2° can be indexed to the (112) plane of the λ1 phase. Compared with the as-homogenized alloy, the diffraction peaks corresponding to the B19′ phase near 43.9° and 45° decrease in intensity after annealing at 500 °C and 600 °C, indicating a variation in the martensitic phase fraction. Similar heat-treatment-sensitive transformation behavior has been reported in high-temperature NiTi(Hf,Zr) systems, where the Hf/Zr ratio and precipitation state regulate the relative stability of B2 and martensitic phases [36]. Meanwhile, the NiZr peak at 38.8° slightly weakens, whereas the diffraction peak of the $(Ti, Zr)_2Ni$ phase at 37.3° becomes more pronounced. This behavior may be attributed to enhanced elemental diffusion during annealing, promoting redistribution of Zr atoms and the formation of $(Ti, Zr)_2Ni$. Thermal exposure of H-phase-strengthened NiTi-20Zr has also been shown to cause obvious phase and microstructural changes associated with precipitation and diffusion [37]. When the annealing temperature increases to 700 °C, strong diffraction peaks corresponding to the B19′ phase are observed at 42.3° and 61.3°, indexed to the (-111) and (022) planes, respectively. A NiZr diffraction peak is also observed at 76.2° with Miller index (080). At 800 °C, the diffraction peak intensity of B19′ at 42.3° further increases, while the B2 peak near 38.4° decreases. This suggests that annealing modifies the phase constitution and transformation characteristics, leading to an increased fraction of martensite at room temperature. In NiTi-based alloys, recovery of dislocations and other processing defects can markedly modify B19′-related transformation behavior, supporting the interpretation that annealing-induced defect reduction contributes to the present phase evolution [38].

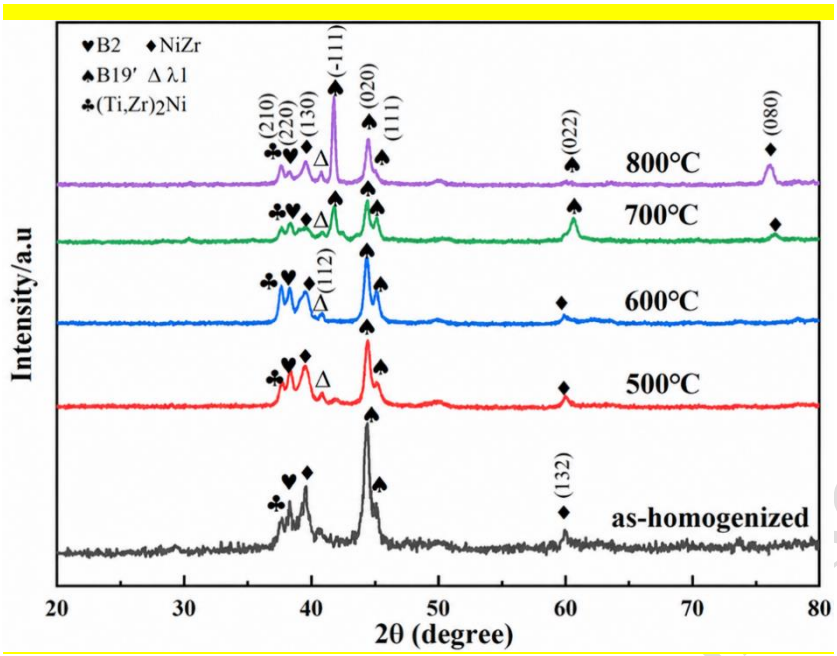

Fig.1 The XRD patterns of the Ni49.5Ti38.5Zr12 alloy in the as-homogenized state and after annealing at different temperatures

Fig. 2 shows the metallographic structure of the Ni49.5Ti38.5Zr12 alloy samples in the as-homogenized state and after annealing at different temperatures. The as-homogenized Ni49.5Ti38.5Zr12 alloy is composed of fine equiaxed grains homogeneously dispersed in the matrix. Small, raised, fibrous martensitic plates are visible on the grain surface. Such plate-like or fibrous surface relief is typical of martensitic variants formed during the B2→B19′ transformation in NiTi-based shape memory alloys. Recent work on NiTi-based ternary alloys further shows that heat-treatment parameters strongly influence phase stability and the visible morphology of transformed regions [39]. After annealing at 500 °C, a large number of raised, plate-like martensitic structures are present within the matrix phase. The fibrous structure of the alloy is significantly reduced, which may be related to stress relaxation, local recovery, and recrystallization during low-temperature annealing. When the annealing temperature is 600 °C, the microstructure exhibits plate-like martensitic variants characteristic of the B19′ phase. The reduction in grain number and the increase in apparent grain size can be attributed to recrystallization and grain-boundary migration. Similar microstructural and functional evolution caused by alloying and heat treatment has been observed in NiTiCu shape memory alloys, indicating that matrix composition and annealing conditions jointly determine martensitic morphology [40]. As the annealing temperature increases further to 700 °C, the fibrous martensitic phase significantly decreases, and the gray λ1 phase, initially observed as isolated small particles, gradually connects into sheet-like structures distributed along grain boundaries or within grains. This indicates that the λ1 phase is closely associated with diffusion-driven segregation and precipitation during annealing. When the annealing temperature reaches 800 °C, the alloy presents fine granular grains that are more uniformly and densely distributed compared with the as-homogenized structure. The gray bubble-like λ1 phase particles are noticeably reduced in size, suggesting that high-temperature annealing promotes further homogenization and partial dissolution/reprecipitation of secondary phases. In related NiTi-based high-temperature alloys, Hf addition has been reported to improve structural stability over a broad temperature range, supporting the role of refractory-element redistribution in stabilizing the annealed microstructure [41].

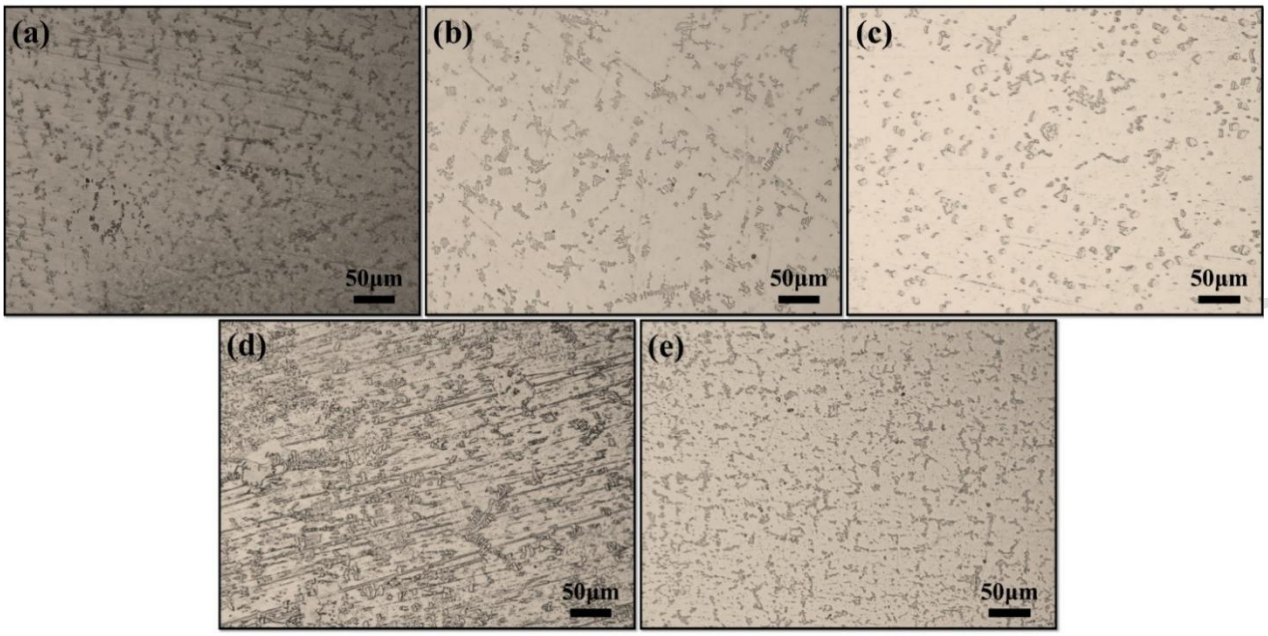

Fig. 2 The metallographic structure of the Ni49.5Ti38.5Zr12 alloy samples in the as-homogenized state and after annealing at different temperatures: (a) as-homogenized, (b) 500 °C, (c) 600 °C, (d) 700 °C, and (e) 800 °C.

Fig. 3 presents the SEM images of the Ni49.5Ti38.5Zr12 alloy samples in the as-homogenized state and after annealing at different temperatures. It can be observed that the microstructure of all the alloys is characterized by a martensitic matrix (dark contrast) and (Ti, Zr)$_2$Ni second phases (black contrast). The contrast difference between matrix and second phases is consistent with precipitation-hardened high-temperature NiTi-based alloys, in which second-phase particles can suppress or locally modify martensitic transformation [42]. After annealing, the λ1 phase is clearly visible in the alloy samples, consistent with the XRD results in Fig. 1. The appearance and evolution of this phase should be understood as a diffusion-controlled second-phase process during annealing, rather than as a direct product of the reversible B2↔B19′ transformation measured by DSC. Recent characterization of designed NiTiHf alloys also confirms that second-phase distribution and matrix composition are key factors controlling microstructure and transformation response [43]. With increasing annealing temperature, the density of defects such as vacancies and dislocations may decrease due to recovery and recrystallization, while local chemical segregation is reduced. When the annealing temperature is excessively high (800 °C), the observed refinement and more compact distribution of second-phase particles may be associated with partial dissolution of coarse precipitates during high-temperature holding and subsequent reprecipitation during cooling. A similar coupling between microstructure and phase transformation has recently been reported in quaternary high-temperature NiTi-based shape memory alloys, further supporting the interpretation that diffusion, precipitation/dissolution, and cooling path jointly determine the final annealed morphology [44].

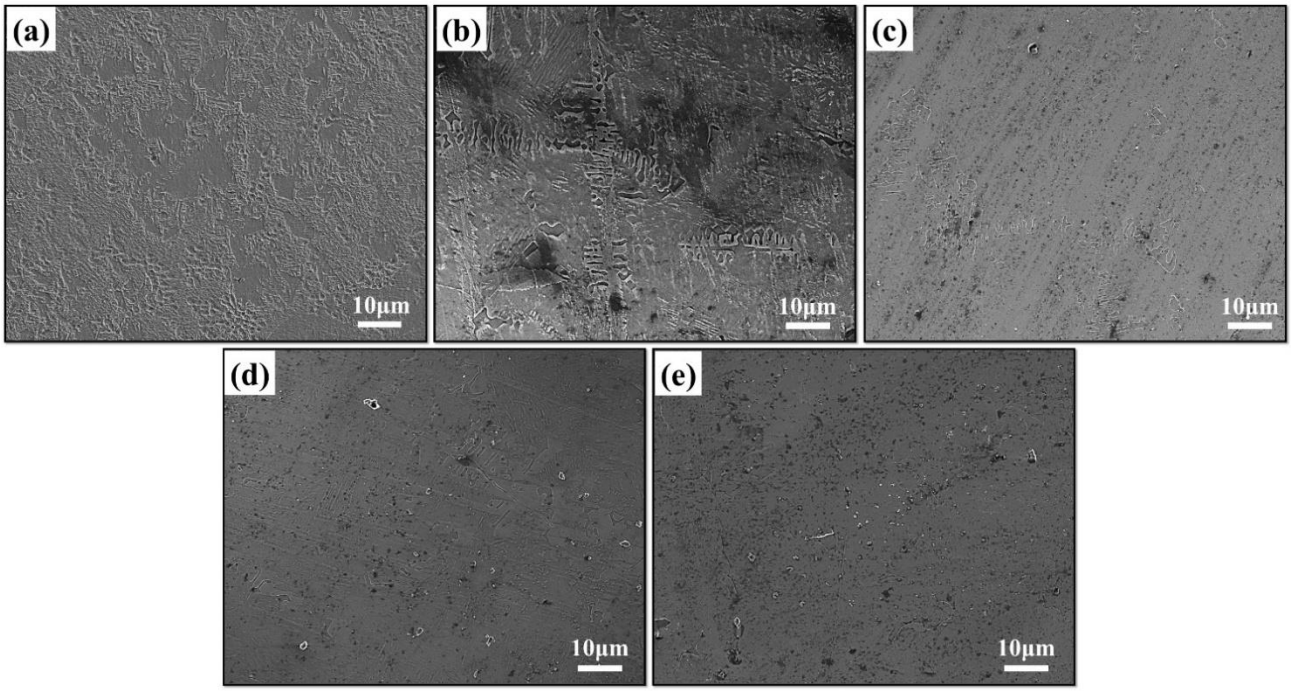

Fig.3 The SEM images of the Ni49.5Ti38.5Zr12 alloy samples in the as-homogenized state and after annealing at different temperatures: (a) as-homogenized, (b) 500 °C, (c) 600 °C, (d) 700 °C, and (e) 800 °C.

Table 1 presents the hardness results of Ni49.5Ti38.5Zr12 alloy samples in the as-homogenized condition and after annealing at different temperatures. As shown in the table, the average microhardness of the as-homogenized sample is 296.6 HV. After annealing at 500 °C, the microhardness increases to 322.9 HV. When the annealing temperature is further raised to 600 °C, the microhardness increases to 355.1 HV, reaching the maximum value. With a further increase in annealing temperature to 700 °C and 800 °C, the microhardness decreases to 347.8 HV and 339.3 HV, respectively. Overall, the microhardness of the alloy after annealing is higher than that of the as-homogenized condition and exhibits a trend of first increasing and then decreasing with increasing annealing temperature. The optimum annealing temperature is 600 °C. This variation is mainly attributed to microstructural evolution and precipitation behavior during the annealing process. In the as-homogenized alloy, compositional segregation and microstructural inhomogeneity may exist, resulting in relatively low hardness. After annealing at 500-600 °C, the microstructure becomes more homogeneous, and fine, dispersed strengthening precipitates may form. The strengthening effect of fine precipitates is consistent with studies on aged Ni-rich NiTi alloys, where precipitation kinetics strongly affect hardness and martensitic transformation behavior [45]. These precipitates effectively hinder dislocation motion, producing a significant precipitation strengthening effect and thereby increasing the microhardness. Surface and near-surface phase formation in heat-treated NiTi also illustrates how local Ni enrichment and second-phase formation can modify mechanical response [46]. When the annealing temperature exceeds 600 °C, the precipitates tend to coarsen or partially dissolve, leading to a reduction in strengthening effectiveness. In addition, high-temperature annealing may result in grain growth, which reduces the grain boundary strengthening effect. The decrease after the hardness peak is therefore consistent with the general effect of precipitation coarsening or phase

instability on strengthening, as reported for Ni_4Ti_3-related martensitic transformation control in NiTi alloys [47]. Under the present experimental conditions, annealing at 600 °C provides the optimal strengthening effect.

Table 1 Presents the microhardness values of the Ni49.5Ti38.5Zr12 alloy samples in the as-homogenized state and after heat treatment at different temperatures.

Temperature (°C)	First	Second	Third	Fourth	Fifth	Average（HV）
as-homogenized	322.2	275.7	285.3	307.6	292.4	296.6
500℃	311.6	336.6	332.1	320.2	321.3	322.9
600℃	357.7	375.4	345.2	365.4	331.8	355.1
700℃	350.7	369.3	347.6	333.4	338.1	347.8
800℃	318.3	373.9	338.5	340.8	325.2	339.3

3.2 Phase Transformation Characteristics

Fig. 4 shows the DSC curves of the alloys. All specimens exhibit clear endothermic and exothermic peaks corresponding to the reversible B2 ↔ B19′ transformation. As listed in Table 2, annealing significantly affects transformation temperatures. After annealing at 500 °C, both As and Af decrease compared with the as-homogenized condition, which may be attributed to partial stress relief and microstructural redistribution. The sensitivity of transformation behavior to particles, local chemistry, and microstructural constraints has recently been emphasized for shape memory alloys, where particles can influence both functional and structural properties [48]. When the annealing temperature increases to 600 °C and above, the transformation temperatures shift toward higher values, reaching Af = 165.4 °C for the 800 °C sample. The transformation enthalpy (ΔH) remains relatively stable at low annealing temperatures but increases noticeably after annealing at 600 °C and above. This increase suggests that a larger fraction of the matrix participates in the reversible martensitic transformation. For NiTi shape memory alloys, latent heat storage capacity is directly associated with the reversible martensitic transformation and is therefore reflected by the DSC enthalpy [49]. The reduction of internal stresses and defect density after recrystallization improves crystallographic compatibility between parent and martensite phases, thereby enhancing transformation reversibility. Recent work on NiTiCu thermal storage alloys also shows that different phase transition behaviors can noticeably change thermal storage response, supporting the connection between the DSC peak, transformation path, and available latent heat [50]. It should be emphasized that ΔH measured by DSC corresponds to the B2-B19′ transformation and is not directly caused by formation of secondary phases during annealing.

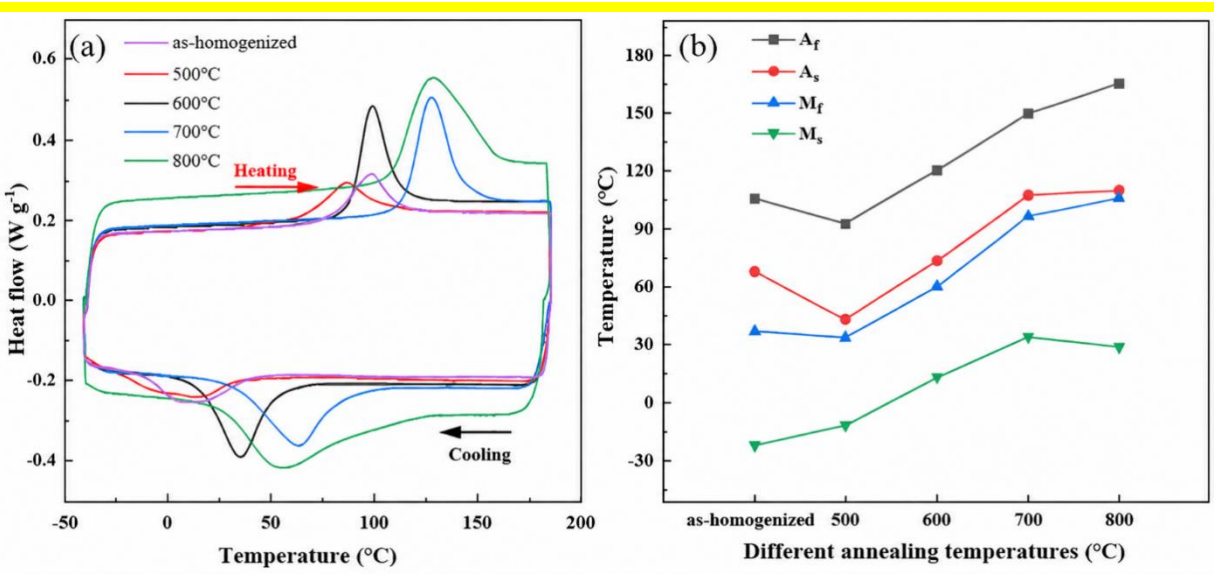

Fig.4 The phase transformation characteristic curves of the Ni49.5Ti38.5Zr12 alloy in the as-homogenized state and after annealing at different temperatures: (a) DSC curves at different annealing temperatures; (b) Phase transformation temperature curves after annealing at different temperatures.

Table 2 presents the phase transformation temperatures and phase transformation enthalpies of the Ni49.5Ti38.5Zr12 alloy in the as-homogenized state and after annealing at different temperatures.

Annealing Temperature (°C)	A_f /°C	A_s /°C	M_s /°C	M_f /°C	ΔH_A /J g^{-1}	ΔH_M /J g^{-1}
as-homogenized	105.3	68.4	35.4	-20.3	22.4	22.1
500°C	93.4	42.5	32.6	-10.8	21.3	20.8
600°C	119.8	72.9	59.7	12.6	29.3	29.2
700°C	149.6	106.4	96.9	32.2	29.6	28.3
800°C	165.4	108	105.7	27.1	30.7	25.9

3.3 Specific Heat Capacity (Cp) and Thermal Conductivity (k)

Based on the previous analysis, it can be seen that the specific heat capacity (Cp) of the alloy increases gradually near the phase transformation temperature, reaches a peak during the phase transformation, and then gradually decreases after the phase transformation is complete. For solid-solid phase-change shape memory alloys, the Cp peak and associated latent heat storage behavior are directly related to the reversible martensitic transformation; NiTiHf alloys have recently been investigated as phase-change thermal storage materials on this basis [51]. The annealing temperature influences the Cp value and distribution by changing the phase transformation temperature, phase transformation range, and microstructure. Fig. 5 shows the specific heat capacity and thermal conductivity of the Ni49.5Ti38.5Zr12 alloy after annealing at different temperatures. From the left axis of Fig. 5, it can be seen that the specific heat capacity of the alloy after different temperature treatments remains nearly constant at room temperature, with a corresponding value of approximately 0.42 $J \cdot g^{-1} \cdot K^{-1}$. When the annealing temperature is 500 °C-600 °C, the specific heat capacity begins to rise sharply at around 70 °C. After reaching the peak, it rapidly decreases, and when the heating

temperature reaches approximately 120 °C, the specific heat capacity drops to 0.5 $J \cdot g^{-1} \cdot K^{-1}$ and stabilizes. When the annealing temperature is 700 °C, the specific heat capacity increases sharply between 100 °C and 170 °C. After reaching the peak, it sharply decreases. It is evident that the alloy treated at this temperature has a slower rate of decrease in specific heat capacity [52].

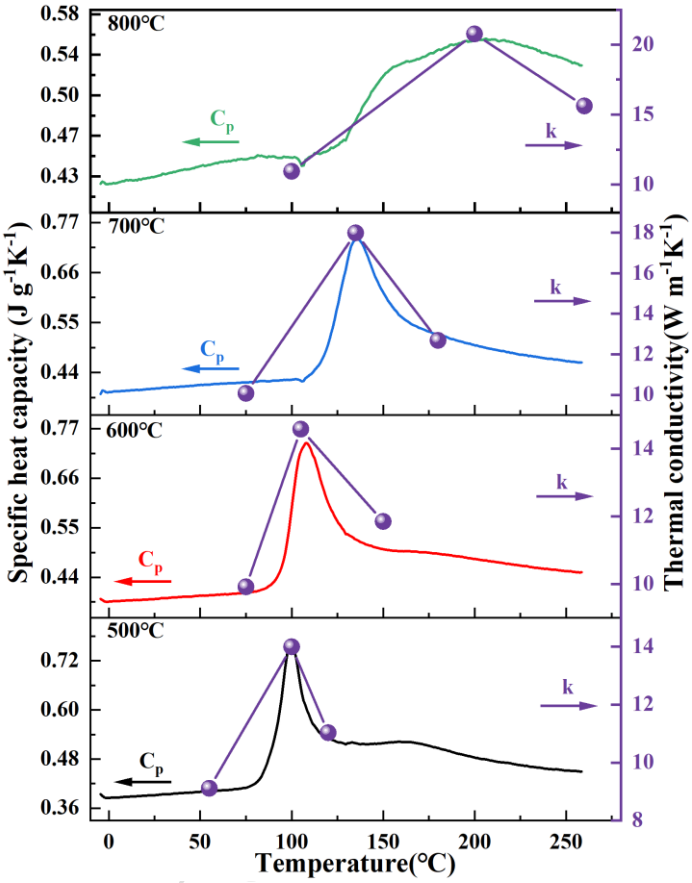

Fig. 5 The specific heat capacity and thermal conductivity of the Ni49.5Ti38.5Zr12 alloy after annealing at different temperatures.

Further increasing the annealing temperature to 800°C significantly slows the rate of increase in specific heat capacity, and the Cp at the peak decreases to 0.55 $J \cdot g^{-1} \cdot K^{-1}$. Although the specific heat capacity at around 260 °C shows a decreasing trend, it does not drop to values close to that at room temperature, which may be due to the narrow temperature range set for the specific heat measurement. Overall, as the annealing temperature increases, the alloy's specific heat capacity peak becomes smoother due to the gradual elimination of internal stresses and defects, and the phase transformation range broadens. This behavior is consistent with the DSC results and can be attributed to the gradual elimination of internal stresses and defects, together with precipitation-induced changes in matrix composition. Grain-growth-induced changes in thermal properties of NiTi alloys have also been reported, indicating that annealing-induced microstructural evolution can modify both transformation and heat-transport behavior [53]. However, excessively high annealing temperatures lead to a certain decrease in the peak value of specific heat capacity.

From the right axis of Fig. 5, it can be seen that the trend in the thermal conductivity of the alloy after annealing at different temperatures is highly consistent with the specific heat capacity. During the phase transformation range, the thermal conductivity first increases and then decreases, and the phase

transformation temperature at the peak typically corresponds to the maximum value of the specific heat capacity. When the annealing temperature was 800 °C, the thermal conductivity reached its peak value of 20.9 $W \cdot g^{-1} \cdot K^{-1}$, which was significantly higher than that of the alloys treated at other annealing temperatures. Overall, as the annealing temperature gradually increases, the thermal conductivity of the alloy shows a gradual upward trend. Combining the microstructure analysis, it can be observed that annealing treatment promotes grain growth, reduces the grain boundary density, and lowers the dislocation density, which in turn facilitates an increase in the alloy's thermal conductivity. During the low-temperature annealing phase (500 - 600 °C), the grains are relatively fine, and there are residual defects from processing, resulting in lower thermal conductivity. As the annealing temperature increases, microscopic defects are further reduced and the microstructure becomes more homogeneous, thus enhancing thermal conductivity. Compositional and microstructural effects have also been shown to control the stability of high-temperature NiTiHf actuation response during repeated thermal-mechanical operation [54]. At 700 °C and 800 °C, the combined effects of grain coarsening, reduced defect density, and changes in phase fraction contribute to the increase in thermal conductivity. However, excessive coarsening or loss of precipitate strengthening may weaken mechanical reliability, as indicated by fatigue-crack-growth studies on precipitate-free and precipitation-hardened NiTiHf alloys [55].

3.4 Thermal Cycling Stability

Based on the phase transformation temperatures discussed earlier, when the annealing temperature is 800 °C, the phase transformation start temperature (As) of the alloy is 108 °C, and the phase transformation finish temperature (Af) is 165.4 °C. This phase transformation range is already higher than the operating temperature of underground electronic devices. Therefore, this section focuses only on the effects of annealing temperatures between 500 °C and 700 °C on the material's thermal cycling stability. Fig. 6 shows the thermal cycling curves and corresponding phase transformation temperatures at different annealing temperatures. From the figure, it can be seen that as the number of thermal cycles increases, both the endothermic and exothermic peaks shift to lower temperatures. Initially, during the first few thermal cycles, the phase transformation temperatures decrease rapidly. After more than 20 cycles, the phase transformation temperature and enthalpy gradually stabilize. This early-cycle shift followed by stabilization is typical of thermal training in high-temperature NiTi-based shape memory alloys, where repeated transformation reduces unstable defects, redistributes internal stress, and stabilizes martensitic variants. Cyclic stability of the two-way shape memory effect in aged NiTiHf polycrystals has likewise been reported to depend strongly on prior thermomechanical treatment and microstructural stabilization [56]. Notably, after 10 thermal cycles, the changes in the alloy's peak values are more pronounced, indicating that most of the microstructural accommodation occurs in the early stage of cycling.For the sample annealed at 500 °C, the changes in As and Ms are 18 °C and 7 °C, respectively. For the sample annealed at 600 °C, the changes in As and Ms are 22 °C and 7 °C, respectively. For the sample annealed at 700 °C, the changes in As and Ms are 10 °C and 5 °C, respectively. Compared with the 500 °C and 600 °C samples, the smaller temperature shift of the 700 °C sample indicates better thermal cycling stability within the tested range.

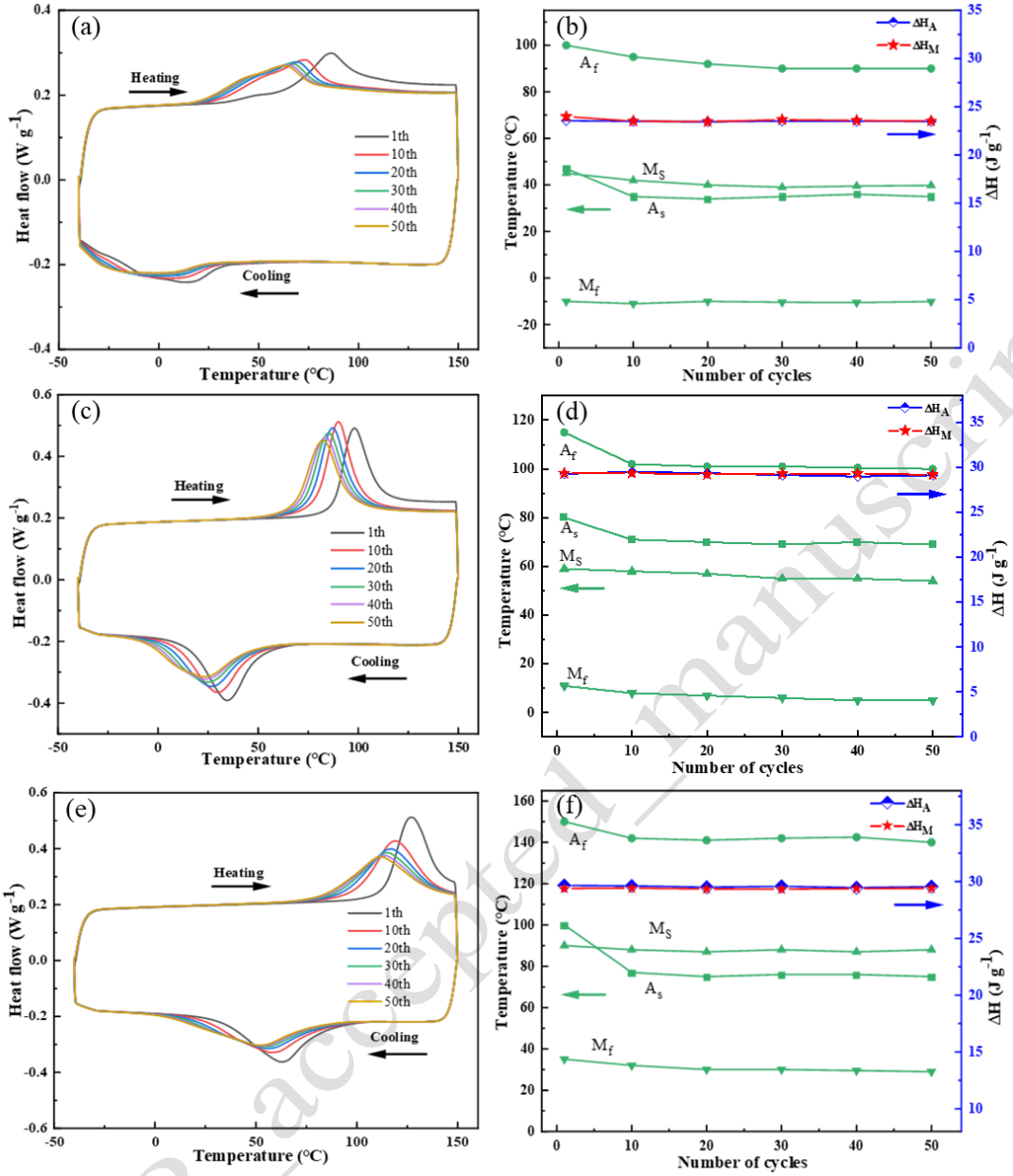

Fig.6 The thermal cycling curves and corresponding phase transformation temperature curves of the Ni49.5Ti38.5Zr12 alloy at different annealing temperatures:(a) Thermal cycling curve at 500 °C (b) Phase transformation temperature curve at 500 °C (c) Thermal cycling curve at 600 °C (d) Phase transformation temperature curve at 600 °C (e) Thermal cycling curve at 700 °C (f) Phase transformation temperature curve at 700 °C

After multiple cycles, the phase transformation enthalpy of the alloy remains nearly constant, indicating that the reversible transformation fraction is not significantly degraded. Functional fatigue studies of NiTi show that repeated cycling can be rapidly characterized by tracking transformation-related heat release and heat absorption, which supports the use of DSC peak evolution as an indicator of cyclic stability [57]. The broader transformation range after annealing can be related to microstructural heterogeneity introduced by second phases and local stress fields. Low-temperature annealing helps repair microscopic defects such as dislocations and vacancies, while higher annealing

temperatures promote grain growth and reduce grain-boundary density, thereby improving thermal cycling stability. However, when the annealing temperature is excessively high, precipitate dissolution, abnormal grain growth, or new defects may reduce cycling stability. Recent studies on transformation-induced structural fatigue further show that repeated phase transformation can introduce damage when microstructural accommodation is insufficient [58]. Therefore, the 600-700 °C range provides a more reasonable balance between transformation temperature and cyclic stability for the present alloy.

4. Conclusions

(1) Annealing temperature significantly influences phase constitution and transformation behavior of Ni49.5Ti38.5Zr12 alloy. Increasing annealing temperature shifts transformation temperatures upward and broadens the transformation interval.

(2) Hardness exhibits a peak value at 600 °C due to precipitation strengthening and microstructural homogenization. Higher temperatures induce grain growth and precipitate coarsening, leading to slight hardness reduction.

(3) Specific heat capacity during transformation increases with annealing temperature, while thermal conductivity improves progressively, reaching ~20.9 W m^{-1} K^{-1} at 800 °C. The enhancement in thermal conductivity is mainly attributed to reduced defect density and grain-boundary scattering.

(4) Thermal cycling tests confirm that annealing within 600-700 °C provides improved transformation stability and nearly constant transformation enthalpy, indicating suitability for high-temperature downhole thermal management applications.

Funding

This work was supported by the General Project of Shaanxi Province Key Research and Development Program (2025CY-YBXM-129).

Author contributions

References

1. Ma J, Xu C, Li M, et al. Experimental study on the flammability limit of associated flammable gases in oil wells under high pressure and temperature[J]. *Journal of Cleaner Production*, 2025, 518: 145943. https://doi.org/10.1016/j.jclepro.2025.145943
2. Lan W, Zhang J, Peng J, et al. Distributed thermal management system for downhole electronics at high temperature[J]. *Applied Thermal Engineering*, 2020, 180: 115853. https://doi.org/10.1016/j.applthermaleng.2020.115853
3. Wei F, Lan W, Deng C, et al. A transient thermal model for forecasting the real-time temperature of downhole electronics[J]. *International Journal of Thermal Sciences*, 2024, 200: 108946. https://doi.org/10.1016/j.ijthermalsci.2024.108946

4. Zhang S, Peng J, Deng C, et al. An integrated downhole thermal management system with improved operating thermal performance and rapid post-operation air cooling[J]. *Applied Thermal Engineering*, 2024, 257: 124473. https://doi.org/10.1016/j.applthermaleng.2024.124473
5. Peng J, Li J, Zhang S, et al. Experimental and numerical investigation on a hybrid high-temperature downhole thermal management system integrating liquid cooling and phase change material[J]. *Applied Thermal Engineering*, 2025, 259: 124804. https://doi.org/10.1016/j.applthermaleng.2024.124804
6. Jin H, Ren S, Zhang Y, et al. Geofluid circulation enhanced downhole heat exchanger for highly efficient heat extraction: Mechanism and optimization[J]. *Geothermics*, 2025, 132: 103424. https://doi.org/10.1016/j.geothermics.2025.103424
7. Zhang Q, Dahi Taleghani A, Elsworth D. Underground energy storage using abandoned oil & gas wells assisted by geothermal[J]. *Journal of Energy Storage*, 2025, 110: 115317. https://doi.org/10.1016/j.est.2025.115317
8. Deng C, Wei F, Peng J, et al. Numerical and experimental study of an integrated thermoelectric active cooling system for ultra-high temperature downhole electronics[J]. *Applied Thermal Engineering*, 2025, 271: 126341. https://doi.org/10.1016/j.applthermaleng.2025.126341
9. Lv Y-G, Chu W-X, Wang Q-W. Thermal management systems for electronics using in deep downhole environment: A review[J]. *International Communications in Heat and Mass Transfer*, 2022, 139: 106450. https://doi.org/10.1016/j.icheatmasstransfer.2022.106450
10. Zhu X, Li S, Dui G, et al. Atomistic study of phase transformation and plastic behaviors of gradient nanocrystalline NiTi shape memory alloy[J]. *European Journal of Mechanics - A/Solids*, 2026, 115: 105838. https://doi.org/10.1016/j.euromechsol.2025.105838
11. Xu B, Yu C, Wang C, et al. Effect of pore on the deformation behaviors of NiTi shape memory alloys: A crystal-plasticity-based phase field modeling[J]. *International Journal of Plasticity*, 2024, 175: 103931. https://doi.org/10.1016/j.ijplas.2024.103931
12. Du C, Li D, Li Y, et al. Ultrafine niobium powder enabled synergetic liquid-phase sintering toward full densification of elemental powder metallurgy NiTi shape memory alloys[J]. *Materials Science and Engineering: A*, 2025, 946: 149090. https://doi.org/10.1016/j.msea.2025.149090
13. Lin G, Jiang L, Hu J, et al. Transient electron properties and phase change in femtosecond laser processing of NiTi alloy: Multiscale simulation and experimental investigation[J]. *Journal of Materials Science & Technology*, 2026, 252: 190 ～ 205. https://doi.org/10.1016/j.jmst.2025.06.025
14. Xie X, Jing C, Xu B, et al. Tunable quasi-linear superelasticity and improved elastocaloric effect of concentration-gradient NiTi alloys via phase-field engineering[J]. *Journal of Materials Research and Technology*, 2025, 39: 7294～7303. https://doi.org/10.1016/j.jmrt.2025.11.077
15. Geng J, Shi Y, Barriobero-Vila P, et al. Ultrastrong and ductile NiTi-based composite with large recoverable strain mediated by a compositionally complex phase[J]. *Applied Materials Today*, 2024, 39: 102347. https://doi.org/10.1016/j.apmt.2024.102347
16. Choi W S, Ko W-S, Park Y, et al. Finely tunable thermal expansion of NiTi by stress-induced martensitic transformation and thermomechanical training[J]. *Acta Materialia*, 2026, 302: 121623. https://doi.org/10.1016/j.actamat.2025.121623
17. Kim J Y, Ryu W-H, Park E S. Manipulation of NiTi-based shape memory alloy nanostructures via a hybrid approach of phase separation and selective leaching[J]. *Materials & Design*, 2025, 259: 114895. https://doi.org/10.1016/j.matdes.2025.114895

18. Gao P, Huang J, Zhang Z, et al. Strain rate effects on deformation and martensitic transformation in NiTi alloys fabricated by additive manufacturing under quasi-static tension[J]. *Journal of Materials Research and Technology*, 2025, 39: 5278 ～ 5286. https://doi.org/10.1016/j.jmrt.2025.10.203
19. Karakoc O, Atli K C, Benafan O, et al. Actuation fatigue performance of NiTiZr and comparison to NiTiHf high temperature shape memory alloys[J]. *Materials Science and Engineering: A*, 2022, 829: 142154. https://doi.org/10.1016/j.msea.2021.142154
20. Qu W, Zhang Q, Li G, et al. Microstructure and thermophysical properties of NiTiZr phase change alloys for downhole tool heat storage[J]. *AIMS Materials Science*, 2025, 12(1): 85～100. https://doi.org/10.3934/matersci.2025007
21. Sun D, Xu H, Zhang J, et al. Achieving high-temperature superelasticity and stable actuation response by nanocrystalline engineering in NiTiZr shape memory alloy[J]. *Scripta Materialia*, 2025, 267: 116836. https://doi.org/10.1016/j.scriptamat.2025.116836
22. Karakoc O, Atli K C, Evirgen A, et al. Effects of training on the thermomechanical behavior of NiTiHf and NiTiZr high temperature shape memory alloys[J]. *Materials Science and Engineering: A*, 2020, 794: 139857. https://doi.org/10.1016/j.msea.2020.139857
23. Evirgen A, Karaman I, Pons J, et al. Role of nano-precipitation on the microstructure and shape memory characteristics of a new Ni50.3Ti34.7Zr15 shape memory alloy[J]. *Materials Science and Engineering: A*, 2016, 655: 193～203. https://doi.org/10.1016/j.msea.2015.12.076
24. Evirgen A, Karaman I, Santamarta R, et al. Relationship between crystallographic compatibility and thermal hysteresis in Ni-rich NiTiHf and NiTiZr high temperature shape memory alloys[J]. *Acta Materialia*, 2016, 121: 374～383. https://doi.org/10.1016/j.actamat.2016.08.065
25. Unni M, Sudagar J. Preparation of electroless deposition of NiTiZr(P) quaternary alloy and their properties[J]. *Heliyon*, 2024, 10(17): e37363. https://doi.org/10.1016/j.heliyon.2024.e37363
26. Vedamanickam S, Vageeswaran P, Jacob B, et al. Prediction of transformation temperatures of NiTiZr shape memory alloys using artificial neural network[J]. *Materials Today Communications*, 2023, 36: 106712. https://doi.org/10.1016/j.mtcomm.2023.106712
27. Wang H, Liang H, Zhang P, et al. Boosted heat dissipation efficiency by sandwich structure containing the thermally conductive segregated network in phase change materials for advanced chip thermal management[J]. *Journal of Energy Storage*, 2025, 133: 117895. https://doi.org/10.1016/j.est.2025.117895
28. Zheng R, Zhou H, Li J. Influence of low melting-point alloy on thermal conductivity and fusion heat of expanded graphite composite shape-stabilized phase change materials[J]. *Journal of Energy Storage*, 2025, 140: 119080. https://doi.org/10.1016/j.est.2025.119080
29. Al-Mahmodi A F, Munusamy Y, Atta M R, et al. Utilizing phase change materials in thermal energy systems: applications in waste heat recovery[J]. *Applied Thermal Engineering*, 2025, 279: 128003. https://doi.org/10.1016/j.applthermaleng.2025.1280
30. Moulakhnif K, El Majd A, Ait Ousaleh H, et al. Thermal performance of shape-stable hydrated salt-based modified diatomite composite phase change materials for low-temperature heat storage[J]. *Solar Energy Materials and Solar Cells*, 2026, 294: 113935. https://doi.org/10.1016/j.solmat.2025.113935
31. Wang X, Chen H, Xu A, et al. Thermal management in cooling pavements: Advancements in harnessing phase change materials to mitigate urban heat island effect[J]. *Journal of Energy Storage*, 2025, 138: 118628. https://doi.org/10.1016/j.est.2025.118628

32. Shi F, He X, Wu W, et al. Study of a composite phase change material with high thermal conductivity and latent heat based on mannitol–dulcitol/MC@rGO[J]. *Chemical Engineering and Processing - Process Intensification*, 2026, 219: 110637. https://doi.org/10.1016/j.cep.2025.110637
33. Kim M, Park D, Kim J. Synergistic integration of porous polymer networks with solid-solid phase change material and surface-modified BN for enhanced thermal conductivity and latent heat storage[J]. *Polymer Testing*, 2025, 151: 108963. https://doi.org/10.1016/j.polymertesting.2025.10896
34. Wang Y, Wang S, Nomura T, et al. Macroencapsulation and in-situ formed Al-Cu-Si ternary alloy phase change materials for high-temperature heat storage[J]. *Solar Energy Materials and Solar Cells*, 2026, 294: 113941. https://doi.org/10.1016/j.solmat.2025.113941
35. Kornegay S M, Kapoor M, Hornbuckle B C, et al. Influence of H-phase precipitation on the microstructure and functional and mechanical properties in a Ni-rich NiTiZr shape memory alloy[J]. Materials Science and Engineering: A, 2021, 801: 140401. https://doi.org/10.1016/j.msea.2020.140401
36. Bigelow G S, Benafan O, Garg A, et al. Effect of Hf/Zr ratio on shape memory properties of high temperature Ni50.3Ti29.7(Hf,Zr)20 alloys[J]. Scripta Materialia, 2021, 194: 113623. https://doi.org/10.1016/j.scriptamat.2020.11.008
37. 37. Oliveira J P, Shen J, Escobar J D, et al. Laser welding of H-phase strengthened Ni-rich NiTi-20Zr high temperature shape memory alloy[J]. Materials & Design, 2021, 202: 109533. https://doi.org/10.1016/j.matdes.2021.109533
38. Vashishtha H, Collins D M. The influence of dislocations on B19′ and R-phase transformations in a NiTi shape memory alloy[J]. Scripta Materialia, 2024, 255: 116365. https://doi.org/10.1016/j.scriptamat.2024.116365
39. Cai S, Schaffer J E, Shi T, et al. Effect of Cu alloying and heat treatment parameters on NiTi alloy phase stability and constitutive behavior[J]. Shape Memory and Superelasticity, 2024, 10: 460-472. https://doi.org/10.1007/s40830-024-00504-x
40. Abdelhady E S, Molotnikov A, Vaneker T, et al. Effect of Cu alloying on the microstructural and functional evolution of NiTiCu shape memory alloys[J]. Shape Memory and Superelasticity, 2026, 12: 97-106. https://doi.org/10.1007/s40830-025-00577-2
41. Li B, Ma Y, Zheng L, et al. Hf addition enhances structural stability and mechanical properties of NiTi alloys across a broad temperature range[J]. Advanced Engineering Materials, 2025, 27(17): 2500712. https://doi.org/10.1002/adem.202500712
42. Hershkovitz E, Yoo T, Gallo F D C, et al. Anisotropic suppression of martensitic transformation in precipitation-hardened NiTiHf high-temperature shape memory alloys[J]. JOM, 2025, 77(5): 2852-2861. https://doi.org/10.1007/s11837-025-07242-0
43. Canadinc D, Breitbach E J, Catal A A. Characterization of two novel NiTiHf shape memory alloys designed by machine learning utilizing novel experimental techniques[J]. Shape Memory and Superelasticity, 2025, 11: 394-407. https://doi.org/10.1007/s40830-025-00551-y
44. Motaharinia N, Nili-Ahmadabadi M, Mohri M. Novel Ni48.5Ti45.5Hf3Ta3 high temperature shape memory alloy: Microstructure and phase transformation[J]. Journal of Alloys and Compounds, 2025, 1042: 183738. https://doi.org/10.1016/j.jallcom.2025.183738
45. 45. Pandolfi G S, Martins S C S, Buono V T L, et al. Precipitation kinetics of Ti3Ni4 and multistage martensitic transformation in an aged Ni-rich Ni-Ti shape memory alloy[J]. Journal of

Materials Research and Technology, 2020, 9(4): 9162-9173. https://doi.org/10.1016/j.jmrt.2020.06.046
46. Freiberg K E, Seyring M, Wonneberger R, et al. Phase formation in the Ni-enriched zone below the surface oxide on NiTi[J]. Intermetallics, 2023, 154: 107817. https://doi.org/10.1016/j.intermet.2022.107817
47. Zhu J, Wu H H, Wu Y, et al. Influence of Ni4Ti3 precipitation on martensitic transformations in NiTi shape memory alloy: R phase transformation[J]. Acta Materialia, 2021, 207: 116665. https://doi.org/10.1016/j.actamat.2021.116665
48. Eggeler G, Frenzel J, Pons J. Particles in shape memory alloys revisited: Effects on functional and structural properties[J]. Shape Memory and Superelasticity, 2025, 11: 350-362. https://doi.org/10.1007/s40830-025-00547-8
49. Kato H. Latent heat storage capacity of NiTi shape memory alloy[J]. Journal of Materials Science, 2021, 56: 8243-8250. https://doi.org/10.1007/s10853-021-05777-6
50. Zuo C, Zheng L, Yang S, et al. Thermal storage properties of NiTiCu shape memory alloys with different phase transition behaviors[J]. Next Materials, 2025, 8: 100577. https://doi.org/10.1016/j.nxmate.2025.100577
51. Hite N, Sharar D J, Trehern W, et al. NiTiHf shape memory alloys as phase change thermal storage materials[J]. Acta Materialia, 2021, 218: 117175. https://doi.org/10.1016/j.actamat.2021.117175
52. Sharar D J, Leff A C, Wilson A A, et al. High-capacity high-power thermal energy storage using solid-solid martensitic transformations[J]. Applied Thermal Engineering, 2021, 187: 116490. https://doi.org/10.1016/j.applthermaleng.2020.116490
53. Warzoha R J, Vu N T, Donovan B F, et al. Grain growth-induced thermal property enhancement of NiTi shape memory alloys for elastocaloric refrigeration and thermal energy storage systems[J]. International Journal of Heat and Mass Transfer, 2020, 154: 119760. https://doi.org/10.1016/j.ijheatmasstransfer.2020.119760
54. Demblon A, Mabe J H, Karaman I. Compositional effects on strain-controlled actuation fatigue of NiTiHf high temperature shape memory alloys[J]. Scripta Materialia, 2024, 242: 115904. https://doi.org/10.1016/j.scriptamat.2023.115904
55. Young B, Orrostieta R, Haghgouyan B, et al. Fracture toughness and fatigue crack growth resistance of precipitate-free and precipitation hardened NiTiHf shape memory alloys[J]. Materials Science and Engineering: A, 2024, 900: 146443. https://doi.org/10.1016/j.msea.2024.146443
56. Panchenko E Y, Marchenko E S, Baigonakova G A, et al. Cyclic stability of two-way shape memory effect in aged Ni50.3Ti32.2Hf17.5 polycrystals after various thermomechanical treatments[J]. Materials, 2023, 16(18): 6175. https://doi.org/10.3390/ma16186175
57. Jury A, Balandraud X, Heller L. Fast characterization of the functional fatigue of NiTi by infrared thermography and heat source reconstruction[J]. Shape Memory and Superelasticity, 2025, 11: 206-229. https://doi.org/10.1007/s40830-025-00537-w
58. Schmelter T, Stötzel N, Versteegen C, et al. Transformation induced structural fatigue of commercial shape memory wires[J]. Shape Memory and Superelasticity, 2025, 11: 494-512. https://doi.org/10.1007/s40830-025-00564-7